Rainbow-color imaging of microbubbles strongly clustering in a turbulent boundary layer

Y. Murai[1,*], D. Saitoh[1], H. J. Park[1], Y. Tasaka[1]
1: Laboratory for Flow Control, Faculty of Engineering, Hokkaido University, Japan
* Correspondent author: murai@eng.hokudai.ac.jp

Keywords: Color imaging, Drag reduction, Turbulent boundary layer, Microbubbles

ABSTRACT

Rainbow-color volumetric illumination for visualizing 3D microbubble distributions was examined in order to find microbubble clustering in a spatially developing turbulent boundary layer. The color coding was defined according to the wall unit from 0 to 200, straddling viscous-sub layer, buffer layer and log-law region. This allowed understanding where the microbubbles were accumulated or diffused within the boundary layer. The results showed microbubble clouding in the low-speed streak regions along the viscous sublayer, clustering into cores of streamwise vortices ejected into the buffer layer, and intermittent exhaust of the clusters toward the log-law region. Furthermore, correlation of these behaviors with local Reynolds shear stress event (ejection, sweep) was found with quadrant analysis of the liquid velocity vector data obtained by PIV.

1. Introduction

In wall turbulence, injection of microbubbles reduces the frictional drag along a solid wall. This is a known fact since the paper by McCormick and Bhattacharyya (1973). [1]. There were reports trying to explain the mechanism of the drag reduction in 1980s with a mathematical model of turbulent boundary layer (Legner, 1984; Marie, 1987). However, it came to an understanding that it should be elucidated as two-phase flow having significant slip between two phases. This propelled experimental reserches in 1990s (Merkle and Deutsch, 1992; Kato et al., 1999; Kodama et al., 2000; Moriguchi and Kato, 2002). Most of these experiments used milli-meter or sub-millimeter sized bubbles, smaller than the boundary layer thickness. For these bubbles, turbulent shear stress in the boundary layer easily enhances complex deformation of bubbles. In 2000-2015, deformability of bubbles was focused by the experimental investigators as a major factor contributing to drag reduction (Kitagawa et al., 2005; van Gils et al., 2013; Tasaka et al., 2015). For real microbubbles, capillary number is sufficiently small because of strong surface tension keeping spherical shape. Question is whether bubble deformation contributes to the drag reduction.

Numerical researchers found an effect of microbubble accumulation into individual vortex cores, which alters the size and the location of the vortices (Ferrante and Elghobashi, 2004). However, point-source approximation of the microbubbles did not simulate volumetric clustering effect of microbubbles. In experimental approaches, most of the papers (Serizawa et al., 2005; Gutierrez-Torres et al., 2008; Hara et al., 2011; Shatat et al., 2009) reported significant effect of such real microbubbles on drag reduction even by the volume fraction was less than 1%. A key to explain the mechanism is to clarify where and how such microbubbles are accumulated and modify the local turbulent eddies inside the boundary layer.

In our experimental study, we have employed a method to visualize 3-D distribution of microbubbles. The method relies on volumetric illumination of microbubbles using a rainbow-type color-coded light applied in a wall proximity. The optical set-up requires only a single camera, allowing effective measurement volume to be kept large enough. A similar technique was reported for tracer particles as the 3-D particle tracking velocimetry (Watamura et al., 2013; Xiong et al., 2019). Our case is to apply the technique for microbubbles which scatters light in a way different from solid particles. A basic principle of the method was reported by the authors previously [Park et al., 2018). In the present paper, we report on the application of the technique combined with PIV analysis for elucidating the inner structure of the turbulent boundary layer altered by the present of microbubbles.

2. Experimental Method

A schematic diagram of experimental facility is shown in **Fig. 1**. It consists of an open water horizontal channel of 3,500 mm in total length and a test plate set vertically in the downstream region of the channel. The recirculation unit is constructed by a pump, a flowmeter, and a bubble separating reservoir tank. The open channel around the test plate is made of transparent acrylic resin for all the three sides to allow various optical visualizations.

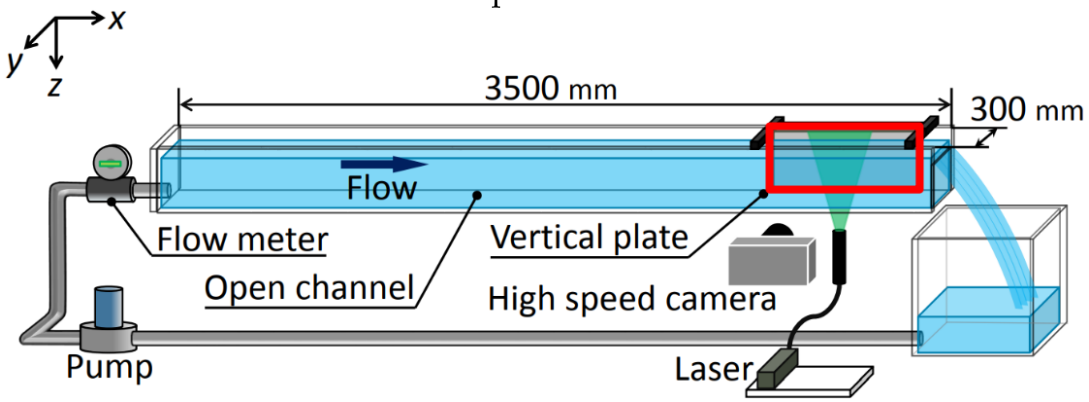

Fig. 1 Open channel for visualizing microbubble-laden flat-plate turbulent boundary layer.

We apply the rainbow illumination to turbulent boundary layer along the test plate in the open channel as illustrated in **Fig. 2a**. Hue value is changed linearly to the distance from the plate surface on the order of red, magenta, blue, cyan, green, yellow and returning to red. Width of the rainbow part is set 12 mm, which is about the boundary layer thickness of the flow. In outer layer at $y > 12$ mm, red monochromatic light is continuously projected so that microbubbles bursting off the boundary layer is identified as red color. An original snapshot of microbubbles image is shown in **Fig. 2b**. Cyan dots in the image correspond to microbubbles flowing in wall proximity at $y < 3$ mm while magenta dots are microbubbles accumulated in turbulent eddies at 4 mm $< y <$ 7 mm. Yellow spots are microbubbles being ejected toward outer layer at 9 mm $< y <$ 12 mm. The exact computation of the depth coordinate of individual microbubbles is performed from measured hue information after opto-geometrical calibration.

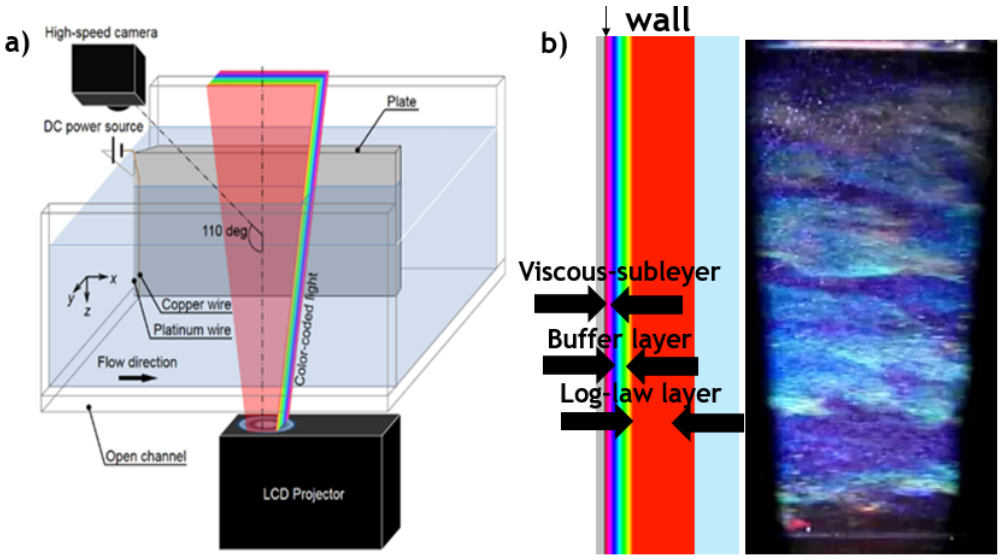

Fig. 2 Microbubble visualization by means of color-coded volumetric illumination. (a) Tangential projection of color-coded light and (b) the color coding of the boundary layer, by which microbubbles reflect corresponding colors.

3. Experimental Results

3-1. Microbubble distribution

By sampling a vertical segment from the high-speed video camera movie, timeline blow up images are generated as shown In **Fig. 3**. In each panel, the horizontal axis indicates time within 5 seconds.

Fig. 4 shows the three-dimensional depiction of the microbubble distribution. Here the position in y-coordinate of individual microbubble was linearly estimated from the hue value (note that the linearity was validated by our previous report (Park et al., 2019)).

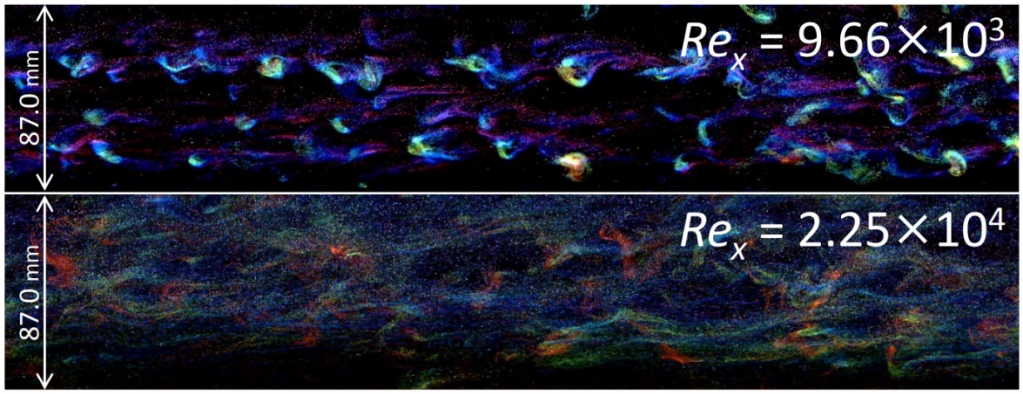

Fig. 3 Time-line blow up image of coloured microbubbles. Top figure is the case of Rex = 9,660 taken in the upstream part of the plate. Bottom figure is that of Rex = 22,500 taken in the downstream part.

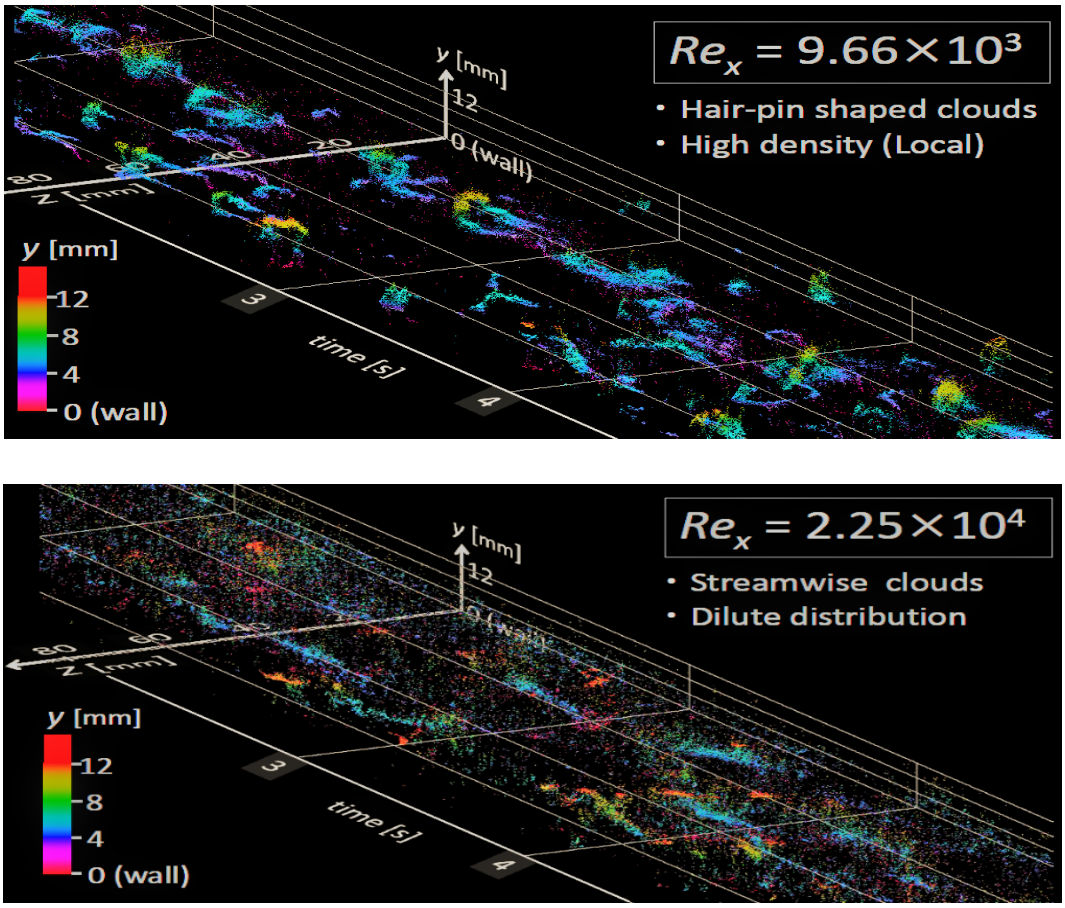

Fig. 4 3-D distribution of microbubbles. (Top) Rex = 9,660 and (Bottom) Rex = 22,500.

3-2. Buffer layer structure

In order to assess how the liquid phase turbulence is modified by the microbubbles, we measured velocity vector of liquid phase with PIV. In parallel to the rainbow illumination for microbubbles,

a laser sheet was illuminated at y = 1.0 mm from the solid wall surface in order to measure the buffer layer structure of liquid phase. Effective thickness of the laser sheet was 1.0 mm. Note that PIV measures approximately the liquid phase flow from motion of microbubbles that have no significant slip from the liquid phase. **Fig. 5** shows a sample of PIV image and its result.

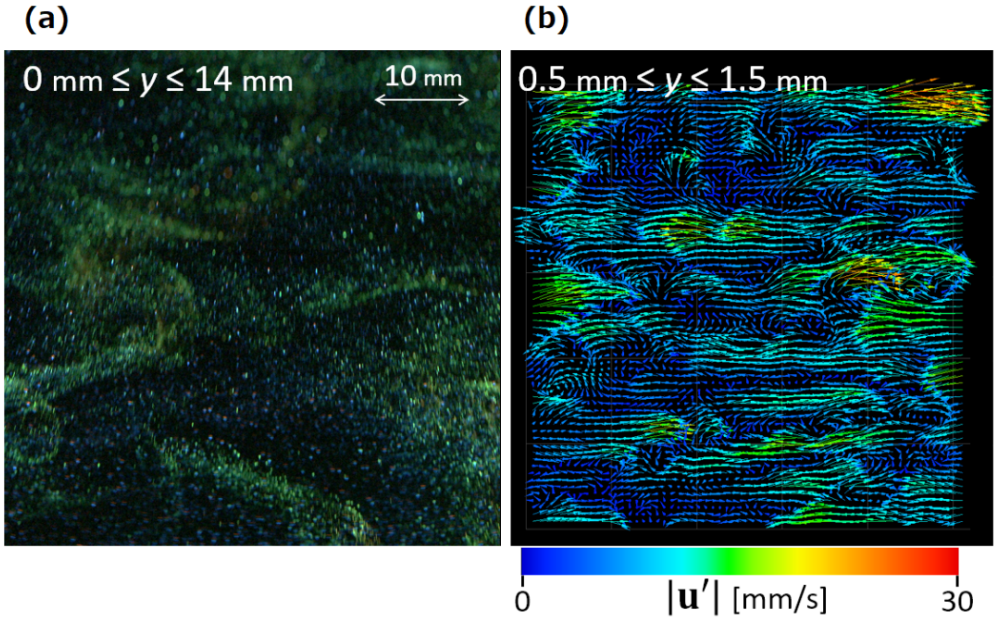

Fig. 5 PIV imaging of microbubbles in the buffer layer. (a) original image and (b) velocity vector obtained by PIV analysis

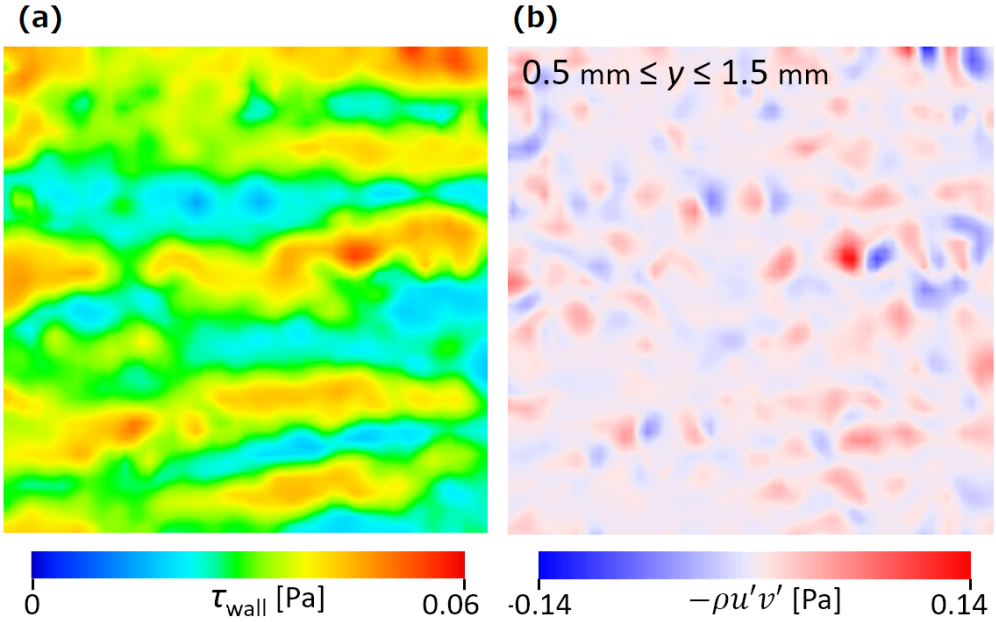

Fig. 6 Instantaneous planar distribution of shear stress. (a) wall shear stress distribution estimated by local velocity gradient and (b) source of Reynolds shear stress

After a long time-series data of PIV was obtained over 2,000 frames, we calculated several quantities that represent turbulent characteristics. **Fig. 6a** shows instantaneous wall shear stress distribution, directly computed from the streamwise velocity gradient assuming local linear shear flow within the viscous sublayer. It clearly demonstrates a spanwise stripe pattern of the wall shear stress, proving formation of low-speed streaks and high-speed sweep regions banded in an integral scale of turbulence. In the same plane, the value of u'v' was obtained as in **Fig. 6b**, which indicates the source of Reynolds shear stress. Here the velocity component perpendicular to the wall, v, was estimated from local equation of continuity integrated in the y direction. The value u'v' has a positive average value (red color) proving that it induces turbulent friction. Blue spots of negative value also appear in the plane, which means reduction of the stress due to microbubbles that are suspended in a form of clouds.

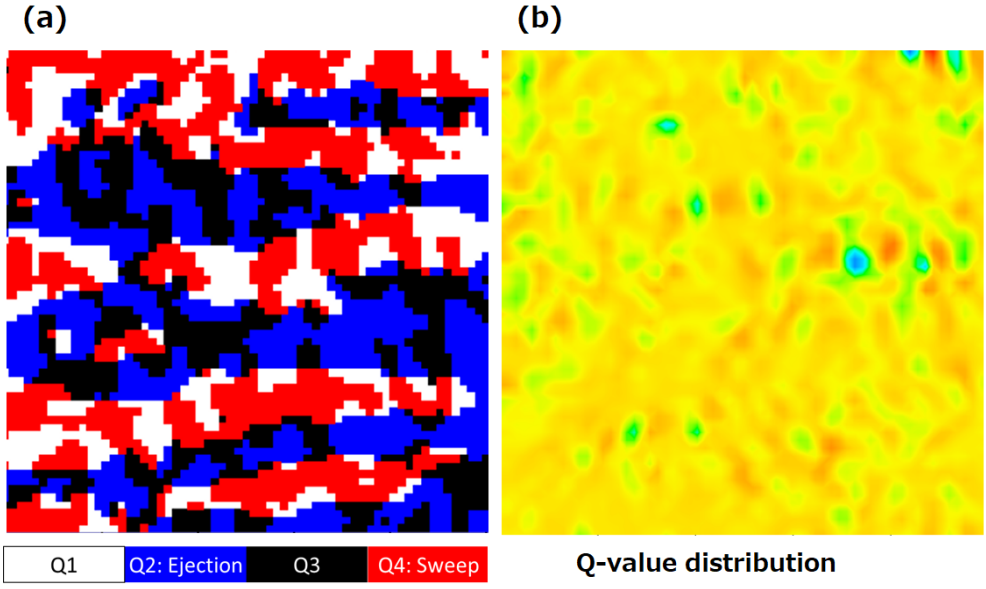

Fig. 7 Visualization of the buffer layer structure altered by presence of microbubbles. (a) quadrant mapping of Reynolds shear stress and (b) distribution of Q-value

The same data of u'v' are re-visualized by **Fig. 7a**, which shows quadrant classification, i.e. Q1 ($u' > 0$, $v' > 0$), Q2 ($u' < 0$, $v' > 0$), Q3 ($u' < 0$, $v' < 0$), and Q4 ($u' > 0$, $v' < 0$). Here, Q2 and Q4 correspond to ejection and sweep, respectively. The result supports that the ejection regions (blue in the figure) are elongated in the streamwise direction having a specific spanwise interval. This is consistent to the formation of low-speed streaks in the viscous sublayer. Sweep regions (red) appear in the non-ejection regions with a local fluctuation. Since all the three velocity components, u, v, and w were measured in the present method, Q-value (second invariant quantity of velocity gradient tensor, or local Laplacian of pressure field) was also analysed as shown in **Fig. 7b**. Mostly the Q-value was obtained positively in the turbulent boundary layer, a few spots of negative value (blue region) take place. This happens unnaturally in the case of single-phase turbulent boundary

layers, and hence it can be regarded as the effect of microbubble clouds. Relationship between the negative Q-value spots and the microbubble clouds is still in the stage of investigation. In our idea, there are two factors to explain the relation: one is strong viscoelasticity of the microbubble clouds, i.e, rheological effect. The other is influence of negative electric charge on the individual microbubble surface in water, which produces Coulomb force to repulse each other as microbubbles form high-number density clouds in the core of turbulent eddies.

To support these ideas, we are now analysing statistic nature of the velocity correlation as shown in **Fig. 8**. In the meantime, we found that the dominancy of ejection and sweep was calmed in the case of microbubble-laden turbulent boundary layer so that turbulent frictional drag can be reduced even though the turbulent intensity itself was unchanged or rather intensified.

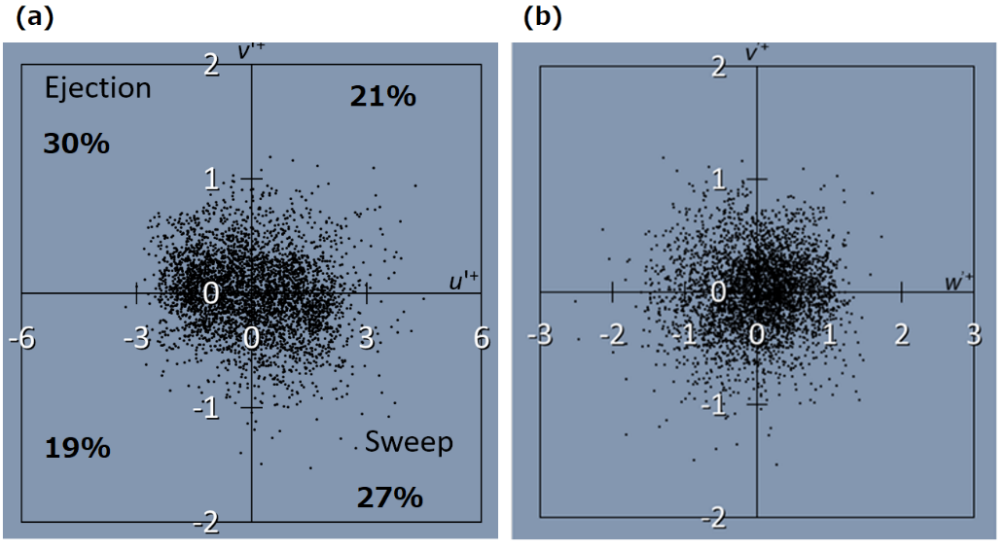

Fig. 8 Correlation of velocity component flucutations. (a) the plane of w'-v' corresponding to sweep/ejection and (b) the plane of w'-v' corresponding to spanwise symmetry

References

Ferrante, A., Elghobashi, S. (2004). On the physical mechanism of drag reduction in a spatially developing turbulent boundary layer laden with microbubbles. *J. Fluid Mech*., 503: 345–355.

Gutierrez–Torres, C. C., Hassan, Y. A., Jimenez–Bernal, J. A. (2008). Turbulence structure modification and drag reduction by microbubble injections in a boundary layer channel flow. *J. Fluids Eng*., 130: 111304.

Hara, K., Suzuki, T., Yamamoto, F. (2011). Image analysis applied to study on frictional drag reduction by electrolytic microbubbles in a turbulent channel flow. *Exp. Fluids*, 50: 715–727.

Kato, H., Iwashina, T., Miyanaga, M., Yamaguchi, H. (1999). Effect of microbubbles on the structure of turbulence in a turbulent boundary layer. *J. Mar. Sci. Tech*., 4: 115–162

Kitagawa, A., Hishida, K., Kodama, Y. (2005). Flow structure of microbubble-laden turbulent channel flow measured by PIV combined with the shadow image technique. *Exp. Fluids*, 38; 466–475

Kodama, Y., Kakugawa, A., Takahashi, T., Kawashima, H. (2000). Experimental study on microbubbles and their applicability to ships for skin friction reduction. *Int. J. Heat Fluid Flow*, 21: 582–588.

Legner, H. H. (1984). Simple model for gas bubble drag reduction. *Phys. Fluids,* 27: 2788–2790.

Marie, J.L. (1987). A simple analytical formulation for microbubble drag reduction. *PhysicoChemical Hydrodynamics*, 8: 213–220

McCormick, M., Bhattacharyya, R. (1973). Drag reduction of a submersible hull by electrolysis. *Nav. Eng. J.*, 85: 11–16.

Merkle, C. L., Deutsch, S. (1992). Microbubble drag reduction in liquid turbulent boundary layers. *ASME Appl. Mech. Rev.*, 45: 103–127.

Moriguchi, Y., Kato, H. (2002). Influence of microbubble diameter and distribution on frictional resistance reduction. *J. Mar. Sci. Tech.*, 7: 79–85.

Park H., Saito, D., Tasaka, Y., Murai, Y. (2019). Color-coded visualization of microbubbles clouds interacting with eddies in a spatially developing turbulent boundary layer, *Exp. Thermal Fluid Sci.*, Vol. 109: 109919.

Park, H., Tasaka, Y., Murai, Y. (2018). Bubbly drag reduction accompanied by void wave generation inside turbulent boundary layers, *Exp. Fluids*, Vol. 59: 164.

Serizawa, A., Inui, T., Eguchi, T. (2005). Flow characteristics and pseudo-laminarization of vertically upward air-water milky bubbly flow with micro bubbles in a pipe. *Jpn. J. Multiphase Flow*, 19: 335–340 (in Japanese).

Shatat, M. M. E., Yanase, S., Takami, T., Hyakutake, T. (2009). Drag Reduction Effects of Micro-Bubbles in Straight and Helical Pipes. *J. Fluid Sci. Tech.*, 4: 156–167.

Tasaka, Y., Kimura, T., Murai, Y. (2015). Estimating the effective viscosity of bubble suspensions in oscillatory shear flows by means of ultrasonic spinning rheometry. *Exp. Fluids*, 56: 1867.

van Gils, D. P. M., Guzman, D. N., Sun, C., Lohse, D. (2013). The importance of bubble deformability for strong drag reduction in bubbly turbulent Taylor–Couette flow. *J. Fluid Mech.*, 722: 317–347.

Watamura, T., Tasaka, Y., Murai, Y. (2013). Intensified and attenuated waves in a microbubble Taylor–Couette flow. *Phys. Fluids*, 25: 054107.

Xiong, J., Idoughi, R., Aguirre–Pablo, A. A., Aljedaani, A. B., Dun, X., Fu, Q., Thoroddsen, S. T., Heidrich, W. (2019), Rainbow particle imaging velocimetry for dense 3D fluid velocity imaging. *ACM Trans. Graph.*, 36: 36.